Cell Reports

Report

Locally Triggered Release of the Chemokine CCL21 Promotes Dendritic Cell Transmigration across Lymphatic Endothelia

Graphical Abstract

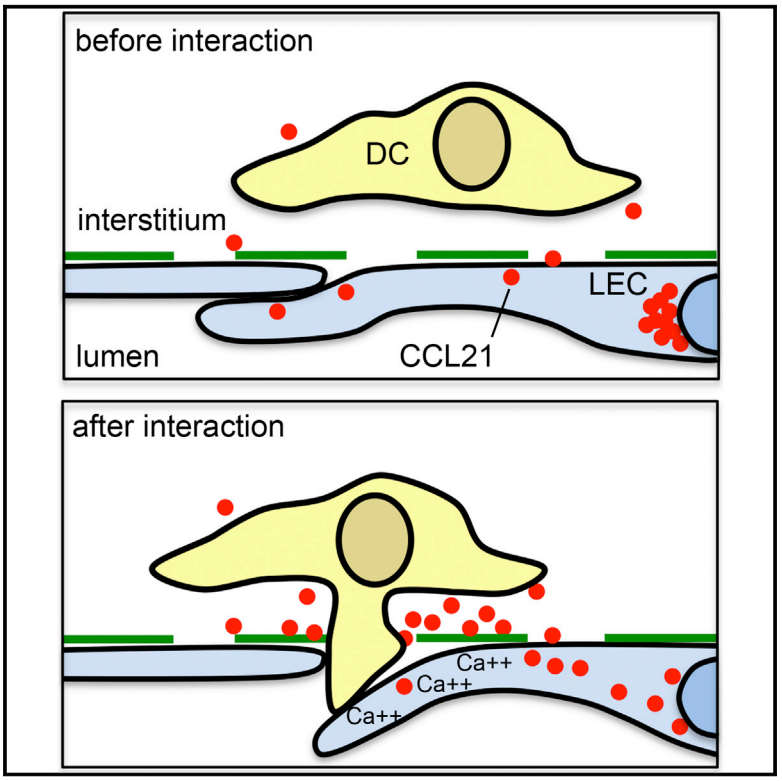

Highlights

- DC entry into lymphatic capillary induces CCL21 secretion to endothelial junctions
- Chemokine CCL21 secretion is triggered by calcium fluxes
- Direct contact by DC induces calcium signaling in LECs
- Dynamic rather than pre-patterned chemokine CCL21 cues promote DC transmigration

Authors

Kari Vaahtomeri, Markus Brown, Robert Hauschild, ..., Matthias Mehling, Walter Anton Kaufmann, Michael Sixt

Correspondence

kari.vaahtomeri@helsinki.fi (K.V.), sixt@ist.ac.at (M.S.)

In Brief

Antigen-presenting dendritic cells approach and enter lymphatic capillaries in a chemokine CCL21-dependent manner. Vaahtomeri et al. show that migrating dendritic cells trigger chemokine-mediated feedback via direct contact with lymphatic endothelia, which locally release CCL21 and thus promote transmigration.

Vaahtomeri et al., 2017, Cell Reports *19*, 902–909
May 2, 2017
http://dx.doi.org/10.1016/j.celrep.2017.04.027

CellPress

OPEN ACCESS
CellPress

Cell Reports
Report

Locally Triggered Release of the Chemokine CCL21 Promotes Dendritic Cell Transmigration across Lymphatic Endothelia

Kari Vaahtomeri,[1,2,*] Markus Brown,[1] Robert Hauschild,[1] Ingrid De Vries,[1] Alexander Franz Leithner,[1] Matthias Mehling,[1] Walter Anton Kaufmann,[1] and Michael Sixt[1,3,*]

[1]Institute of Science and Technology Austria (IST Austria), Am Campus 1, 3400 Klosterneuburg, Austria

[2]Wihuri Research Institute and Translational Cancer Biology Program, Research Program Unit, University of Helsinki, Biomedicum Helsinki, Haartmaninkatu 8, 00290 Helsinki, Finland

[3]Lead Contact

*Correspondence: kari.vaahtomeri@helsinki.fi (K.V.), sixt@ist.ac.at (M.S.)

http://dx.doi.org/10.1016/j.celrep.2017.04.027

SUMMARY

Trafficking cells frequently transmigrate through epithelial and endothelial monolayers. How monolayers cooperate with the penetrating cells to support their transit is poorly understood. We studied dendritic cell (DC) entry into lymphatic capillaries as a model system for transendothelial migration. We find that the chemokine CCL21, which is the decisive guidance cue for intravasation, mainly localizes in the *trans*-Golgi network and intracellular vesicles of lymphatic endothelial cells. Upon DC transmigration, these Golgi deposits disperse and CCL21 becomes extracellularly enriched at the sites of endothelial cell-cell junctions. When we reconstitute the transmigration process in vitro, we find that secretion of CCL21-positive vesicles is triggered by a DC contact-induced calcium signal, and selective calcium chelation in lymphatic endothelium attenuates transmigration. Altogether, our data demonstrate a chemokine-mediated feedback between DCs and lymphatic endothelium, which facilitates transendothelial migration.

INTRODUCTION

Endothelial and epithelial monolayers and their associated basement membranes form physical and functional barriers separating distinct tissue compartments. These barriers are frequently breached, e.g., by immune cells as part of their homeostatic or inflammatory trafficking, by tumor cells during metastatic spread, or during tissue reorganizations in development. Although such transmigration events do not follow one stereotypic pattern, certain mechanisms recur. First, often the migrating cell is guided toward the barrier by extracellular guidance cues such as chemokines. Second, adhesion of the migrating cell to the barrier is mediated by sequential cell-cell interactions, as exemplified in the leukocyte extravasation cascade (Reymond et al., 2013; Vestweber, 2015). Third, transmigration across the barrier usually occurs via entry portals, which may either be developmentally regulated (Nourshargh et al., 2010; Seifert and Lehmann, 2012) or induced by the migrating cell itself (Nourshargh et al., 2010; Vestweber, 2015).

Despite their apico-basal asymmetry, endothelia, and epithelia are often penetrated in both directions: e.g., neutrophils usually extravasate blood vessels from luminal to interstitial but can also transmigrate in the reversed direction (intravasation) (Woodfin et al., 2011). Likewise, tumor cells intravasate blood vessels upon leaving the primary tumor and extravasate to colonize distant organs (Reymond et al., 2013). Hence, rather than acting as pre-patterned gradients, which stereotypically guide the cells across the barrier, the directional cues governing transmigration might act locally and dynamically.

Lymphatic endothelial cells (LECs) of the lymphatic capillaries form a barrier for intravasating leukocytes and tumor cells. Dendritic cells (DCs) enter these vessels on their way from the periphery to the lymph nodes, where DCs activate lymphocytes as part of the adaptive immune response (Förster et al., 2008). DCs are guided from the interstitium toward the lymphatic capillaries by gradients of the chemokine CCL21 (Weber et al., 2013), which is homeostatically secreted by the LECs (Nakano and Gunn, 2001). After arrival at the lymphatic capillary, DCs penetrate the basement membrane (Pflicke and Sixt, 2009) and the LEC junctions (Baluk et al., 2007). The molecular mechanisms directing DCs into the vascular lumen, which we investigate here, are largely unclear.

RESULTS AND DISCUSSION

CCL21 Is Mobilized upon Interactions between Dendritic Cells and Lymphatic Endothelia

DCs are attracted to the vicinity of lymphatic capillaries via gradients of CCL21 (Weber et al., 2013). Notably, CCL21 immunostainings in non-permeabilized tissues show a very faint interstitial signal compared to a strong signal localizing to LECs in permeabilized tissues (Johnson and Jackson, 2010; Tal et al., 2011; Weber et al., 2013). These depots are observed as perinuclear puncta (Johnson and Jackson, 2010; Weber et al., 2013), which co-stain for the Golgi marker GOLPH4 (Figure 1A)

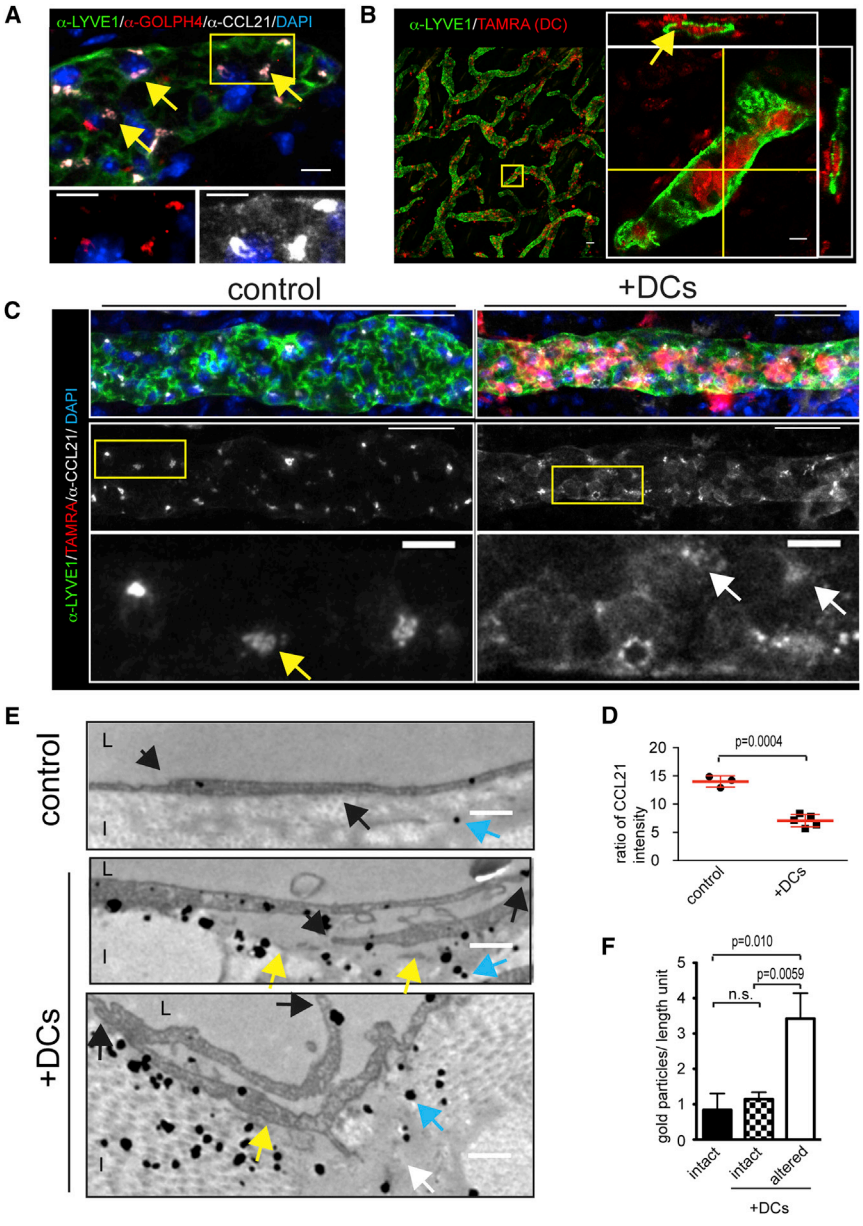

Figure 1. Dendritic Cell Entry into Mouse Dermal Lymphatic Capillaries Induces Mobilization of CCL21

(A) Mouse dermal lymphatic capillary stained for LYVE1 (green), GOLPH4 (red), CCL21 (white), and nuclei (DAPI, blue). Yellow arrows indicate co-localization of CCL21 and Golph4. Zoom-in of boxed area is shown below.

(B) TAMRA-labeled DCs (red) and LYVE1-stained lymphatic capillaries (green) after 3 hr 30′ invasion. Yellow lines indicate the plane of orthogonal section, and yellow arrow highlights a transmigration event.

(C) LYVE1 (green), CCL21 (white), and nuclei (DAPI, blue) of the ear dermis after 3 hr 30′ in presence or absence (control) of TAMRA-labeled DCs (red). Bottom image shows zoom-in of boxed area. White arrows indicate dispersion of CCL21 (yellow arrow in control).

(D) Dot blot graph shows ratio of signal in high intensity CCL21 depots to CCL21 in other areas of LECs. Columns represent mean values ± SD of control (n = 3) and + DC (n = 5) samples of ~300 μm long lymphatic vessel stretches.

(E) Transmission electron micrograph of CCL21 staining of dermis. Black arrows indicate overlapping LEC tips at cell-cell junctions, yellow arrow detachment of LECs from interstitial extracellular matrix, white arrow rearrangement of collagen bundles, and blue arrow a silver-amplified CCL21 Immunogold label.

(F) Quantification of extracellular CCL21 staining at sites of DC-associated tissue alterations (see E) compared to intact area in same sample or sample devoid of DCs. Bar graph shows mean ± SD of two (–DC) and four (+DC) independent ear samples. Scale bars, 10 μm (A); 50 μm (B and C); 10 μm in zoom-in images; and 500 nm (E).

See also Figure S1.

and disperse upon Golgi-endoplasmic reticulum (ER) disrupting Brefeldin A treatment (Weber et al., 2013). In addition to these *trans*-Golgi depots, CCL21 locates to intracellular vesicles (Figures 1A and S1A) (Johnson and Jackson, 2010), which might represent chemokine en route to homeostatic secretion or stores for "on demand" release. To test if intravasation of DCs changes CCL21 distribution, we layered in vitro-generated DCs on mouse ear explants. In this setup, DCs enter the tissue within minutes and migrate along gradients of interstitial CCL21 to ultimately intravasate into the dermal lymphatic vessels (Pflicke and Sixt, 2009; Weber et al., 2013; Weber and Sixt, 2013) (Figure 1B). In lymphatic capillaries, which had been entered by many DCs, we found that perinuclear CCL21 depots were dispersed and overall diminished (Figures 1C and 1D). This change in CCL21 distribution was not observed at sites where few DCs intravasated or in ears loaded with DCs deficient for the CCL21 receptor CCR7 (Figure S1B). *Ccr7*$^{-/-}$ DCs cannot read the interstitial CCL21 gradient and therefore do not interact with the lymphatic capillaries (Förster et al., 1999; Ohl et al., 2004; Weber et al., 2013).

To study whether mobilization of CCL21 upon DC intravasation was associated with extracellular CCL21 enrichment, we employed immunometal transmission electron microscopy. In line with the immunofluorescence analysis (Figure 1A), intracellular CCL21 was found enriched in the nuclear periphery (Figure S1C) and, more sparsely, in intracellular vesicles of control samples (Figure S1D). Extracellular CCL21 was mostly detected within 1 μm distance of the basolateral side of LECs with no evidence of CCL21 gradients extending from the basolateral to the luminal side of the LECs (Figure 1E). In samples exposed to DCs, local presence of DCs was associated with poorly organized interstitial collagen and partial detachment of the LECs from

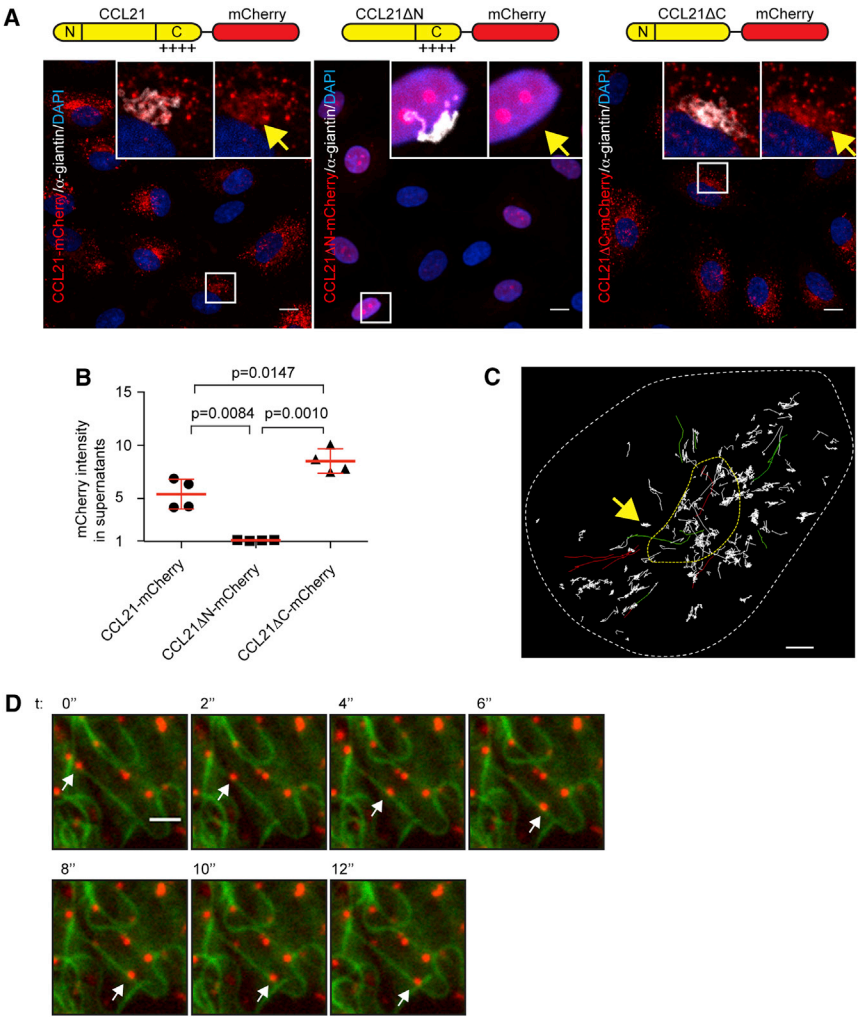

Figure 2. CCL21-Positive Vesicles Localize to Golgi-Secretory Pathway and Traffic along Microtubules

(A) Giantin (white) and nuclear staining (DAPI, blue) of CCL21-mCherry (red), CCL21ΔN-mCherry, or CCL21ΔC-mCherry expressing LECs. Insets show Golgi localized mCherry signal (yellow arrows) with or without staining of Golgi marker giantin.

(B) Quantification of mCherry intensities in supernatants of CCL21-mCherry, CCL21ΔN-mCherry, and CCL21ΔC-mCherry expressing LECs. Dot blot graph shows a mean ± SD of pooled data from two independent experiments, n = 4 for each construct. Intensities are normalized to media background, which is set as 1.

(C) Basolateral non-directed tracks of TIRF-imaged CCL21-mCherry-positive vesicles are indicated with white, directed tracks heading toward Golgi area with green, directed tracks toward cell periphery with red, the Golgi apparatus with a dashed yellow line, and the boundaries of cell contact surface with dashed white line. Yellow arrow indicates a white trajectory representing random movement within a confined area.

(D) TIRF imaging of CCL21ΔC-mCherry (red) and EGFP-tubulin-α (green) expressing primary LEC. White arrow highlights one CCL21ΔC-mCherry positive vesicle (red) throughout the image series. See Movie S1. Scale bars, 10 μm (A); 2 μm (C and D). See also Figure S2.

the interstitium (Figures 1E, S1E, and S1F). Importantly, these signatures of DC intravasation were associated with extracellular accumulations of basolateral, but not luminal, CCL21 (Figure 1E-1F). These accumulations were most prominent at LEC-LEC junctions of detached endothelia (Figure 1E), whereas sheer proximity of DCs seemed insufficient to discharge chemokine (Figure S1G). Based on these findings, we hypothesize that contact between DCs and LECs triggers acute CCL21 secretion. Triggered exocytosis of chemokine is reminiscent of exocytotic targeting of the adhesion molecule PECAM to areas of lymphocyte transmigration at the blood endothelium (Mamdouh et al., 2003). It might provide local guidance or act as a landmark for following DCs, which have been shown to intravasate with increased efficiency (Martin-Fontecha et al., 2003).

CCL21 Leaves the Golgi Apparatus via Microtubules

To directly study CCL21 secretion, we established a traceable in vitro setup, where we lentivirally expressed variants of CCL21 in human dermal LECs, which recapitulated localization to the Golgi secretory pathway (compare Figures 2A and S1A) (de Jong et al., 2005, 2008). Secretion of CCL21 into the cell culture supernatant was dependent on the N-terminal signaling peptide (Figures 2A and 2B). Surprisingly, exclusion of the CCL21ΔN-mCherry from the secretory pathway led to nuclear localization, possibly owing to a potential bipartite nuclear localizing signal in mature CCL21 (aa 21–50). The loss of the heavily cationic C terminus (CCL21ΔC) did not affect localization to the Golgi secretory pathway (Figure 2A) but instead prevented binding of CCL21 to the cell culture dish surface (Figure S2A) and lead to increased CCL21 in the cell culture supernatant (Figure 2B). This was in line with previous findings, showing that the C terminus immobilizes CCL21 to charged surfaces and glycosaminoglycans (Hirose et al., 2002).

To trace the intracellular trafficking routes of CCL21, we performed real-time total internal reflection fluorescence (TIRF) microscopy. Tracking of CCL21-mCherry-positive vesicles showed two modes of behavior: some vesicles rapidly advanced along linear trajectories, whereas others moved randomly within confined areas (Figure 2C). Linear tracks connected Golgi area and the LEC periphery (Figure 2C), matching the distribution pattern of microtubules (Figure S2B). Accordingly, CCL21 was microtubule-associated as revealed by immunostaining of untagged CCL21 and CCL21ΔC (Figure S2B) and live imaging of CCL21ΔC-mCherry (Figure 2D; Movie S1). Microtubule disruption by nocodazole abolished the component of directed movement (Movie S1) confirming that CCL21 is transported along microtubules, which is analogous to the

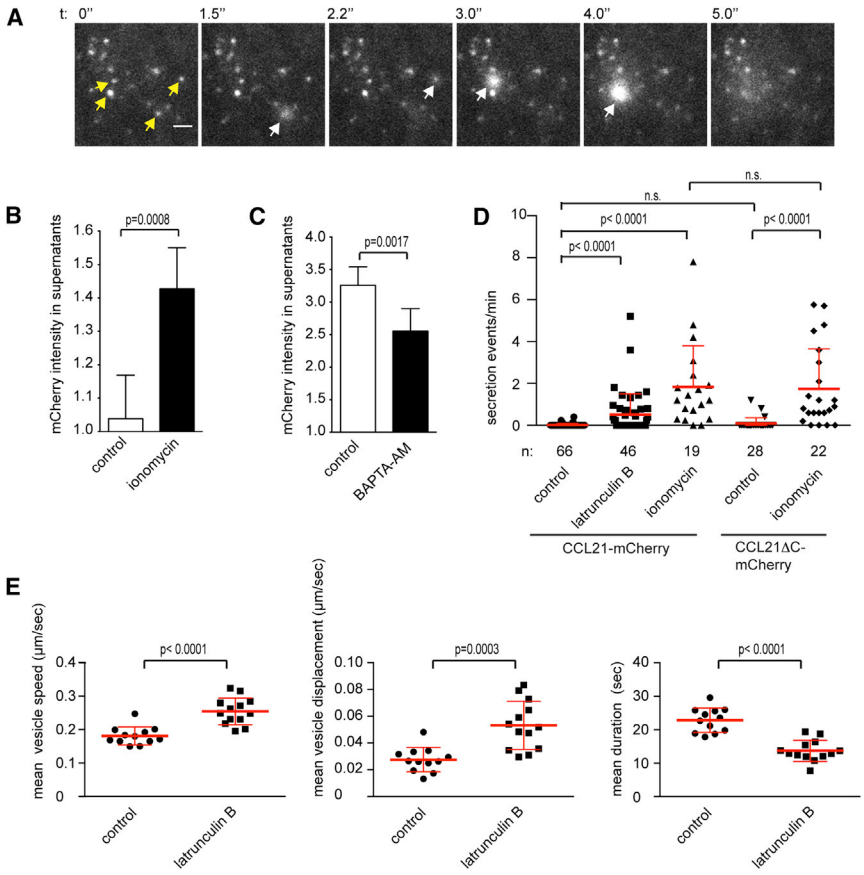

Figure 3. Regulation of CCL21 Secretion

(A) TIRF microscopy of CCL21-mCherry vesicles (white) of a single LEC after addition of 5 μM ionomycin. Yellow arrows indicate vesicles at time point 0″, secretion events are highlighted by white arrows. Scale bar, 2 μm. See Movie S2.

(B) Quantification of mCherry intensities of CCL21ΔC-mCherry expressing LEC culture supernatant subsequent to 6′ control or 5 μM ionomycin treatment. Bar graph shows mean ± SD of pooled samples from 3 independent experiments, n = 5 (control) and 6 (ionomycin).

(C) Quantification of mCherry intensities of culture supernatants of CCL21ΔC-mCherry expressing LECs 4 hr after washout of 1 hr long control or 10 μM BAPTA-AM treatment. BAPTA-AM is a cell-permeant Ca chelator, which is trapped in cells and binds intracellular calcium via carboxylic acid functional groups thus severely decreasing intracellular-free calcium. Bar graph shows mean ± SD of pooled samples from three independent experiments, n = 7 for each condition. Intensities of (B) and (C) are normalized to media background, which is set as 1.

(D) Quantification of pooled data from all TIRF experiments on single vesicle secretion. Data points show secretion frequency in control, 5 μM ionomycin-, or 500 ng/mL latrunculin B-treated CCL21-mCherry or CCL21ΔC-mCherry expressing single LECs as indicated in the figure. The dot blot graph shows mean ± SD secretion frequency in pooled data of single cells from 6 independent experiments, cell number (n) is indicated in the figure.

(E) Data points show CCL21-mCherry vesicle speed, displacement, and duration in the TIRF imaging plane (basolateral membrane) in control and 13 latrunculin B (500 ng/mL)-treated single LECs, which displayed highest CCL21 secretion (see Figure 3D latrunculin B column). The dot blot graph shows mean ± SD of vesicle tracks (51–513/cell) in pooled data of single cells (n = 12 for control and 13 for latrunculin B) of three independent experiments. See Movie S3.

transport of insulin in secretory pancreatic beta-cells (Boyd et al., 1982; Varadi et al., 2003). Similarly to insulin, some of the linear trajectories of CCL21 vesicles were directed toward the cell periphery and some toward the Golgi area, suggesting regulation of vesicle dwell time at the LEC periphery (Zhu et al., 2015).

CCL21 Secretion Is Regulated by Calcium and Cortical Actin

TIRF imaging revealed that occasionally CCL21-mCherry vesicles were discharged into the extracellular space. Regulated discharge of plasma membrane-docked vesicles is often initiated by calcium (Ca) binding to synaptotagmins, which triggers the actual membrane fusion event (Südhof, 2012). Accordingly, the Ca ionophore ionomycin triggered robust CCL21-mCherry and CCL21ΔC-mCherry secretion as directly observed with TIRF microscopy as a sudden and transient increase in CCL21 intensity (Figures 3A and 3D; Movie S2). Such flashes are due to the exponential increase in TIRF signal once the quantum of fluorescent probe enters the glass-water interface below the cell (Axelrod, 1981), which is then followed by rapid dilution of the radially diffusing probe. Bulk mCherry signal in the LEC culture supernatant was increased by ionomycin (Figure 3B). Further, basal secretion seemed at least partially dependent on Ca as chelation of intraendothelial Ca with BAPTA-AM causing a 30% reduction in CCL21ΔC-mCherry secretion (Figure 3C).

Ionomycin did not trigger secretion of all plasma membrane-associated vesicles (Movie S2). Some of these vesicles might not be plasma membrane-docked, but rather sequestered within the cortical actin meshwork, which has to be penetrated before the vesicles can directly contact the membrane (Nakata and Hirokawa, 1992; Oheim and Stühmer, 2000; Giner et al., 2007). When we visualized the cortical actin meshwork of LECs with Lifeact-EGFP, lateral movements similar to that of CCL21-mCherry vesicles were apparent (Movie S3). Actin disassembly by latrunculin B substantially increased the frequency of secretion events (Figure 3D; Movie S3), likely because of enhanced contact between vesicles and secretory machinery. Accordingly, the LECs displaying latrunculin B-induced secretion showed increased movement of vesicles in the basolateral plane as well as in z-direction (revealed by disappearance of vesicles from the TIRF field) (Figure 3E; Movie S3). These results suggest that the cortical actin meshwork controls CCL21 secretion by restricting membrane-docking of vesicles.

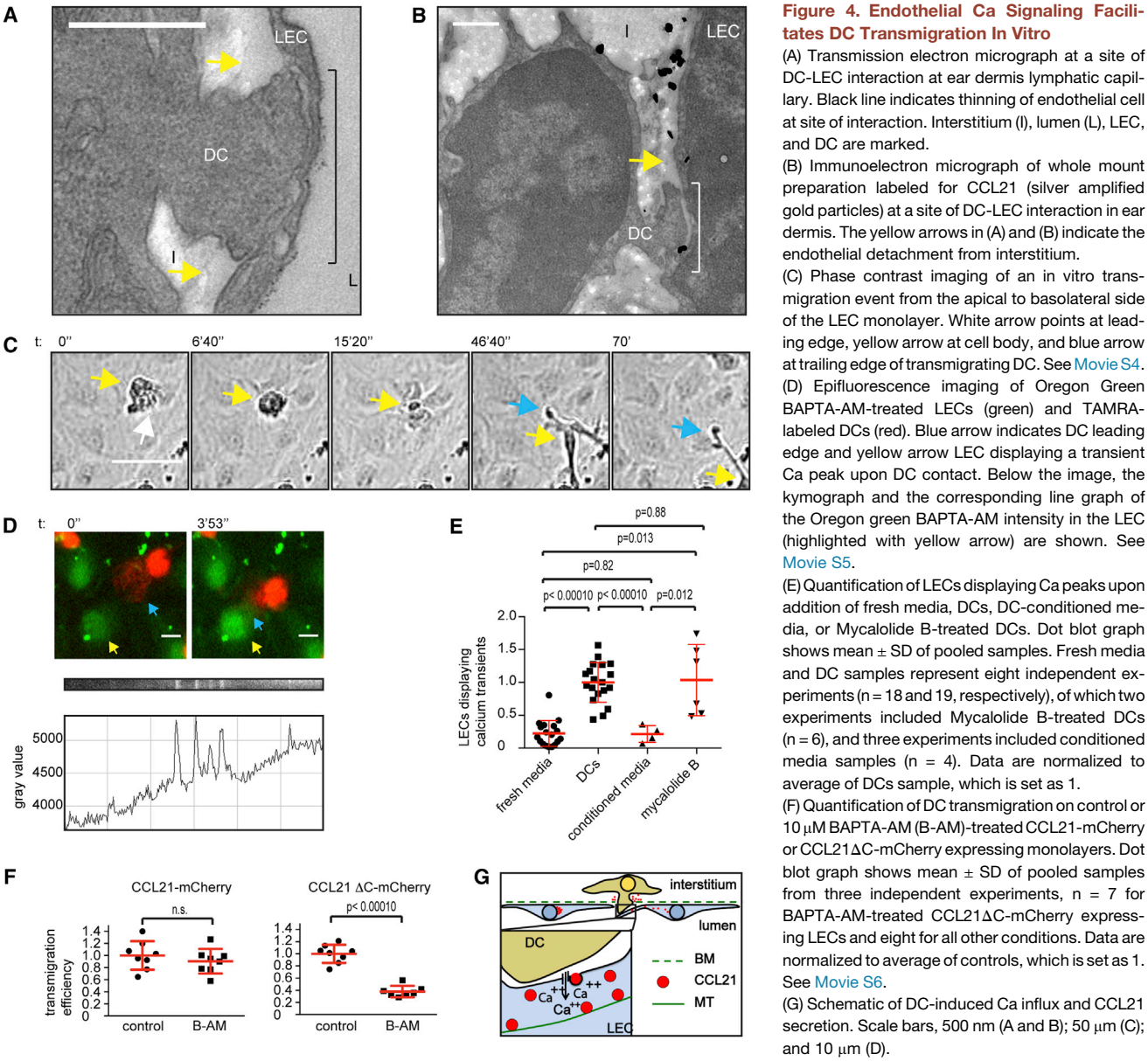

Figure 4. Endothelial Ca Signaling Facilitates DC Transmigration In Vitro

(A) Transmission electron micrograph at a site of DC-LEC interaction at ear dermis lymphatic capillary. Black line indicates thinning of endothelial cell at site of interaction. Interstitium (I), lumen (L), LEC, and DC are marked.

(B) Immunoelectron micrograph of whole mount preparation labeled for CCL21 (silver amplified gold particles) at a site of DC-LEC interaction in ear dermis. The yellow arrows in (A) and (B) indicate the endothelial detachment from interstitium.

(C) Phase contrast imaging of an in vitro transmigration event from the apical to basolateral side of the LEC monolayer. White arrow points at leading edge, yellow arrow at cell body, and blue arrow at trailing edge of transmigrating DC. See Movie S4.

(D) Epifluorescence imaging of Oregon Green BAPTA-AM-treated LECs (green) and TAMRA-labeled DCs (red). Blue arrow indicates DC leading edge and yellow arrow LEC displaying a transient Ca peak upon DC contact. Below the image, the kymograph and the corresponding line graph of the Oregon green BAPTA-AM intensity in the LEC (highlighted with yellow arrow) are shown. See Movie S5.

(E) Quantification of LECs displaying Ca peaks upon addition of fresh media, DCs, DC-conditioned media, or Mycalolide B-treated DCs. Dot blot graph shows mean ± SD of pooled samples. Fresh media and DC samples represent eight independent experiments (n = 18 and 19, respectively), of which two experiments included Mycalolide B-treated DCs (n = 6), and three experiments included conditioned media samples (n = 4). Data are normalized to average of DCs sample, which is set as 1.

(F) Quantification of DC transmigration on control or 10 μM BAPTA-AM (B-AM)-treated CCL21-mCherry or CCL21ΔC-mCherry expressing monolayers. Dot blot graph shows mean ± SD of pooled samples from three independent experiments, n = 7 for BAPTA-AM-treated CCL21ΔC-mCherry expressing LECs and eight for all other conditions. Data are normalized to average of controls, which is set as 1. See Movie S6.

(G) Schematic of DC-induced Ca influx and CCL21 secretion. Scale bars, 500 nm (A and B); 50 μm (C); and 10 μm (D).

See also Figure S2.

DCs Induce Lymphatic Endothelial Ca Fluxes via Cell-Cell Contact

The finding that Ca influx triggers CCL21 secretion in LECs (Figures 3A, 3B, and 3D; Movie S2) together with our in situ finding that DCs cause release of CCL21 (Figures 1E and 1F) suggested that DC-LEC interactions might induce Ca signals in LECs similar to Ca signals in blood endothelia when being transmigrated by polymorphonuclear leukocytes (Huang et al., 1993). While Ca signaling can be induced in several ways, we were struck by our in situ observation of DCs probing LECs with a blunt foot-like processes (Figures 4A and 4B), which were reminiscent of lymphocyte processes physically penetrating blood endothelium (Carman et al., 2007; Shulman et al., 2011). DC protrusions considerably deformed LECs and even detached them locally from the underlying extracellular matrix (Figures 4A, 4B, S1E, and S1F). This suggested that DCs exert pushing forces on LECs, which might promote communication via extended cell-cell contacts. To investigate whether direct interaction was required for Ca signals, LECs were grown to confluency, and DCs were layered on top. In this setting, DCs effectively transmigrated the monolayer (Maddaluno et al., 2009) as revealed by phase contrast live cell imaging (Figure 4C; Movie S4). Transmigration was dependent on the secretion of CCL21, as non-infected or CCL21ΔN-mCherry-infected LECs were only occasionally penetrated by DCs (Figure S2D; Movie S4). Importantly, DCs interacting with the apical side of LECs and DCs in transit through the monolayer induced an increase in Ca concentration in LECs as revealed by time-lapse imaging of a Ca sensor

(Figure 4D; Movie S5). At the population level, LECs showed a low basal frequency of Ca transients, which was increased 4.5-fold upon addition of DCs (Figure 4E). Unlike DCs, DC-conditioned media did not induce an increase in Ca concentration (Figure 4E) excluding a major role for secreted factors. Further, pre-treatment of DCs with Mycalolide B, an irreversible actin depolymerizing agent (Hori et al., 1993; Saito et al., 1994), which prevents formation of actin-based cell protrusions, did not abolish Ca transients (Figure 4E). These results suggest that molecular engagements at the DC-LEC interface are sufficient triggers. Earlier, DC expressed β2 integrins (LFA-1) and its lymphatic endothelial ligand ICAM have been shown to be necessary for in vivo and in vitro transmigration of inflamed but not homeostatic endothelia, where ICAM is not expressed (Johnson et al., 2006; Johnson and Jackson, 2010; Vigl et al., 2011; Teijeira et al., 2013). Accordingly, β2 integrins were dispensable for the DC entry into the dermal lymphatic capillaries as shown before (Figure S2E) (Lämmermann et al., 2008). At sites of intravasated β2 deficient (*Itgb2*$^{-/-}$) DCs, CCL21 depots were dispersed from Golgi similar to wild-type DC samples (Figures S2E and S2F). Thus, other molecular interactions at the DC-LEC interface, such as the plexin1A-semaphorin3A axis (Takamatsu et al., 2010), L1 (Maddaluno et al., 2009), or yet unidentified factors might trigger the signal.

DC-Stimulated Lymphatic Endothelial Ca Fluxes Facilitate Transendothelial Migration

To directly investigate whether lymphatic endothelial Ca signaling was necessary for the transendothelial migration of DCs, we selectively chelated endothelial Ca with BAPTA-AM. We compared the responses to both CCL21-mCherry and CCL21ΔC-mCherry, because full-length CCL21-mCherry accumulates on the cell culture dish surface (Figure S2A), which is not seen in vivo (Figure 1E). Thus, we presumed that the truncated chemokine more faithfully mimics the in vivo situation. Both CCL21-mCherry and CCL21ΔC-mCherry supported transmigration but Ca chelation reduced the number of transmigration events only in CCL21ΔC-mCherry expressing monolayers (62.4% reduction, Figure 4F; Movie S6), which lack the unphysiological accumulation of CCL21 (see Figure S2A) and thus lack a prepatterned CCL21 gradient across the monolayer (similarly to the tissue context, Figure 1E). These results suggest that DCs induce a transient Ca signal in LECs, which triggers acute CCL21 secretion and possibly enables opening of the endothelial junctions, as described for blood endothelia (Huang et al., 1993).

Although the decisive role of chemokines in leukocyte extravasation is well established, it has remained unclear if and how chemokines act during the actual transmigration process. Our finding that CCL21 is acutely secreted upon contact between DCs and LECs extend data by Shulman et al. (2011), which suggested that the chemokine CCL2 is released by blood endothelia in response to interactions with extravasating lymphocytes. While we show that a direct DC-LEC contact is sufficient to trigger chemokine release even in the absence of cytoskeletal force generation (Figure 4E), we found that applying mechanical pushing forces on LECs, and thus increasing LEC plasma membrane tension (Apodaca, 2002), can also trigger Ca flux and CCL21 release in vitro (Figures S2G–S2I). This was in line with the observation that transmigrating DCs considerably deformed LECs in dermal tissue (Figures 4A and 4B) and might suggest that molecular and mechanical triggers perpetuate the intravasation process in concert.

Earlier, long range CCL21 gradients were shown to guide DCs to the vicinity of lymphatic vessels (Weber et al., 2013). However, LEC penetration could not be explained by a simple concentration gradient across the endothelium as intra-luminal CCL21 concentrations are lower than those on the abluminal basement membrane (Weber et al., 2013; Russo et al., 2016). The acute chemokine release that we demonstrate exposes the leading edge of DCs to a burst of very steep CCL21 gradient, which will likely "motivate" the cell to locally push into the endothelium. At sites of loose button-like LEC-LEC junctions (Baluk et al., 2007), physical pushing might open the junction and allow entry from the confined interstitial environment into the lymphatic capillary lumen where physical resistance is lower (Figure 4G). In addition, local chemokine release might boost transmigration by attracting more transmigrating cells toward the specific entry portal, or provide local guidance and thereby determine the actual site of penetration. Taken together, our data show that the barrier cells take a more active role in their penetration than previously anticipated.

EXPERIMENTAL PROCEDURES

Mice

Wild-type C57BL/6J (Charles River Laboratories), *Ccr7*$^{-/-}$ (Förster et al., 1999) and *Itgb2*$^{-/-}$ (Wilson et al., 1993) male and female mice were bred and maintained according to the local rules (Institutional Review Board approval 66018/3-II/3b/2010). Mice were sacrificed at the age of 6–8 weeks for the ear preparation and at the age of 8–12 weeks for the bone marrow extraction.

Ear Sheet Preparation and Explant DC Intravasation Assay

Ears of sacrificed mice were prepared as previously described (Weber et al., 2013). Ear sheets were fixed with 4% paraformaldehyde (PFA) in PBS at room temperature for 25′ or prepared for the DC lymphatic capillary intravasation assay as follows: the ventral half of the ear was mounted between a 0.5 mL microcentrifuge tube lid and the body of the tube, of which the lower part was cut off. The 1.5 cm^2 well formed by the cut tube was filled with 200 μL of R10 with or without 50,000 (Figures 1B–1F) or 100,000 (Figures S2E and S2F) TAMRA-labeled DCs. Unattached DCs were washed off with R10 after 30′ incubation at +37°C and 5% CO_2 and incubated in R10 for additional 1–3 hr (Figures 1B–1F). As *Itgb2*$^{-/-}$ DCs are slower in invading ear explants, *Itgb2*$^{-/-}$ DCs and wild-type controls were kept on the ear explants for 7 hr (i.e., for the whole duration of the experiment) (Figures S2E and S2F). The experiments were terminated by washing the ear once with PBS followed by fixation with 4% PFA in PBS at room temperature for 25′.

CCL21 Quantification in Transmission Electron Microscopy

For the quantification of extra-LEC CCL21, we used two independent samples devoid of DCs (control) and four independent samples with DCs (+DCs). Each sample contained two to five lymphatic vessels. All extracellular CCL21-immunometal particles within 1 μm distance to the interstitial (basolateral) side of the lymphatic vessel endothelial cell were quantified. The particles were classified based on their location either in the intact area or in the area displaying DC-associated tissue alterations (i.e., disorganized collagen bundles and/or local detachment of LECs from the interstitial extracellular matrix). Finally, the particle number was normalized to the corresponding endothelial length.

Measurements of mCherry Signals of the Culture Supernatant

The bulk secretion of CCL21 was measured by analyzing mCherry intensities in the culture supernatant. To measure the amounts of CCL21-mCherry,

CCL21ΔN-mCherry, and CCL21ΔC-mCherry (Figure 2B), culture supernatant was collected 48 hr after full confluency of the LEC culture and the last media change. For the experiments shown in Figure 3, we used CCL21ΔC-mCherry because it has low affinity to culture substrate (Figure S2A), and the changes in secretion should be immediately reflected in the mCherry intensity in the supernatant. Here, culture supernatant was collected subsequent to 6′ 5 μM ionomycin (Molecular Probes), 4 hr after washout of 1 hr 10 μM BAPTA-AM (Life Technologies, B6769) treatment or corresponding control (DMSO) treatments. Results were normalized to the background fluorescence of the MV2 culture media. For the information on measurement and quantification (Figure 2B), see the Supplemental Experimental Procedures.

Live TIRF Imaging of CCL21-mCherry-Positive Vesicles

Ionomycin (final concentration 5 μM, Molecular Probes) was added to the CCL21-mCherry expressing LECs and imaging was started 10 s later whereas latrunculin B (500 ng/mL, Merck Millipore 428020) and nocodazole (500 nM, Sigma, m1404) were added on the LECs 30′ prior to imaging. Vesicle tracks were analyzed with Imaris (Bitplane). Averages of all the tracks/cell, which lasted for longer than 2.5 s, are shown in Figure 3E. The basolateral secretion events were quantified from acquired movies by using FiJi software. Only events in which the vesicles were observed prior to the "flash" and vesicle-like signal was severely decreased or totally absent after the flash were quantified as a secretion event (Figure 3D).

In Vitro DC Transmigration Assay

Activated DCs were centrifuged (300RCF, 5′) and resuspended in MV2 (Promocell) culture media. A total of 40,000 DCs (CCL21ΔC-mCherry monolayers; Figures 4F and S2D; Movie S4) were added on 1.5 cm^2 well of days 4–5 confluent LECs. Due to more efficient transmigration of DCs on CCL21-mCherry monolayers in comparison to CCL21ΔC-mCherry monolayers, DC number was reduced to 25,000 for Figure 4F CCL21-mCherry monolayers. The acquired movies were quantified for the number of DCs beneath the monolayer at 1 hr for CCL21-mCherry or at 3 hr for CCL21ΔC-mCherry expressing LEC monolayers (Figure 4F; Movie S6). For quantification of transmigration efficiency on non-infected or CCL21-mCherry full-length or mutant construct expressing LEC monolayers (Figure S2D), a percentage of transmigrated DC of all DCs was determined.

LEC Ca Sensor Assays

For the Ca-sensor assays, fresh media, DC-conditioned media, or either TAMRA-labeled non-treated or Mycalolide B-treated DCs were carefully added on LEC monolayers treated for 50′ with 10 μM Oregon Green BAPTA-AM. The time-lapse imaging was started after 10′. For the cell population analysis (Figure 4E), imaging lasted for 10′ and the number of LECs displaying transient Ca peaks was quantified from acquired videos. All the Ca sensor experiments were carried out in the absence of serum or added growth factors. See the Supplemental Experimental Procedures for detailed protocol.

Statistics

Prism5 and Prism6 software (GraphPad softwares) was used to test the normality of the data (D'Agostino and Pearson omnibus normality test or Kolmogorov-Smirnov normality test) and for subsequent parametrical t test (two-tailed with Welch's correction) or non-parametrical Mann-Whitney tests. Figure legends indicate number of independent experiments and biological replicates (n) used for statistical analysis.

Other Procedures

Generation and labeling of DCs, ear sheet staining, preparation of transmission electron microscopy samples, construction of lentiviral expression plasmids, virus production, LEC culture and infections, LEC staining, microscopy setups, mechanical pushing of the LECs, image analysis, and identification of putative nuclear localizing signal in CCL21 are outlined in the Supplemental Experimental Procedures.

SUPPLEMENTAL INFORMATION

Supplemental Information includes Supplemental Experimental Procedures, two figures, and six movies and can be found with this article online at http://dx.doi.org/10.1016/j.celrep.2017.04.027.

AUTHOR CONTRIBUTIONS

K.V. and M.S. conceived experiments and wrote the manuscript. K.V., M.B., R.H., I.D.V., M.M., and W.A.K. performed experiments. W.A.K. directed design of electron microscopy experiments. A.F.L. provided lentiviral LifeAct plasmid and dendritic cell cultures. K.V. analyzed the data. K.V. and R.H. performed Imaris analysis. R.H. wrote image analysis scripts.

ACKNOWLEDGMENTS

We thank Tea Vallenius and Matyas Fendrych for critical reading of the manuscript. This work was supported by a Sigrid Juselius Foundation fellowship (K.V.), a post-doctoral research grant from the Academy of Finland (287853 to K.V.), by the European Research Council (ERC GA 281556 to M.S.), and by the Austrian Science Foundation (FWF) (Y564-B12 START award to M.S.).

Received: December 7, 2016
Revised: March 21, 2017
Accepted: April 10, 2017
Published: May 2, 2017

REFERENCES

Apodaca, G. (2002). Modulation of membrane traffic by mechanical stimuli. Am. J. Physiol. Renal Physiol. *282*, F179–F190.

Axelrod, D. (1981). Cell-substrate contacts illuminated by total internal reflection fluorescence. J. Cell Biol. *89*, 141–145.

Baluk, P., Fuxe, J., Hashizume, H., Romano, T., Lashnits, E., Butz, S., Vestweber, D., Corada, M., Molendini, C., Dejana, E., and McDonald, D.M. (2007). Functionally specialized junctions between endothelial cells of lymphatic vessels. J. Exp. Med. *204*, 2349–2362.

Boyd, A.E., 3rd, Bolton, W.E., and Brinkley, B.R. (1982). Microtubules and beta cell function: effect of colchicine on microtubules and insulin secretion in vitro by mouse beta cells. J. Cell Biol. *92*, 425–434.

Carman, C.V., Sage, P.T., Sciuto, T.E., de la Fuente, M.A., Geha, R.S., Ochs, H.D., Dvorak, H.F., Dvorak, A.M., and Springer, T.A. (2007). Transcellular diapedesis is initiated by invasive podosomes. Immunity *26*, 784–797.

de Jong, E.K., Dijkstra, I.M., Hensens, M., Brouwer, N., van Amerongen, M., Liem, R.S.B., Boddeke, H.W.G.M., and Biber, K. (2005). Vesicle-mediated transport and release of CCL21 in endangered neurons: a possible explanation for microglia activation remote from a primary lesion. J. Neurosci. *25*, 7548–7557.

de Jong, E.K., Vinet, J., Stanulovic, V.S., Meijer, M., Wesseling, E., Sjollema, K., Boddeke, H.W.G.M., and Biber, K. (2008). Expression, transport, and axonal sorting of neuronal CCL21 in large dense-core vesicles. FASEB J. *22*, 4136–4145.

Förster, R., Schubel, A., Breitfeld, D., Kremmer, E., Renner-Müller, I., Wolf, E., and Lipp, M. (1999). CCR7 coordinates the primary immune response by establishing functional microenvironments in secondary lymphoid organs. Cell *99*, 23–33.

Förster, R., Davalos-Misslitz, A.C., and Rot, A. (2008). CCR7 and its ligands: balancing immunity and tolerance. Nat. Rev. Immunol. *8*, 362–371.

Giner, D., López, I., Villanueva, J., Torres, V., Viniegra, S., and Gutiérrez, L.M. (2007). Vesicle movements are governed by the size and dynamics of F-actin cytoskeletal structures in bovine chromaffin cells. Neuroscience *146*, 659–669.

Hirose, J., Kawashima, H., Swope Willis, M., Springer, T.A., Hasegawa, H., Yoshie, O., and Miyasaka, M. (2002). Chondroitin sulfate B exerts its inhibitory effect on secondary lymphoid tissue chemokine (SLC) by binding to the C-terminus of SLC. Biochim. Biophys. Acta *1571*, 219–224.

Hori, M., Saito, S., Shin, Y.Z., Ozaki, H., Fusetani, N., and Karaki, H. (1993). Mycalolide-B, a novel and specific inhibitor of actomyosin ATPase isolated from marine sponge. FEBS Lett. *322*, 151–154.

Huang, A.J., Manning, J.E., Bandak, T.M., Ratau, M.C., Hanser, K.R., and Silverstein, S.C. (1993). Endothelial cell cytosolic free calcium regulates neutrophil migration across monolayers of endothelial cells. J. Cell Biol. *120*, 1371–1380.

Johnson, L.A., and Jackson, D.G. (2010). Inflammation-induced secretion of CCL21 in lymphatic endothelium is a key regulator of integrin-mediated dendritic cell transmigration. Int. Immunol. *22*, 839–849.

Johnson, L.A., Clasper, S., Holt, A.P., Lalor, P.F., Baban, D., and Jackson, D.G. (2006). An inflammation-induced mechanism for leukocyte transmigration across lymphatic vessel endothelium. J. Exp. Med. *203*, 2763–2777.

Lämmermann, T., Bader, B.L., Monkley, S.J., Worbs, T., Wedlich-Söldner, R., Hirsch, K., Keller, M., Förster, R., Critchley, D.R., Fässler, R., and Sixt, M. (2008). Rapid leukocyte migration by integrin-independent flowing and squeezing. Nature *453*, 51–55.

Maddaluno, L., Verbrugge, S.E., Martinoli, C., Matteoli, G., Chiavelli, A., Zeng, Y., Williams, E.D., Rescigno, M., and Cavallaro, U. (2009). The adhesion molecule L1 regulates transendothelial migration and trafficking of dendritic cells. J. Exp. Med. *206*, 623–635.

Mamdouh, Z., Chen, X., Pierini, L.M., Maxfield, F.R., and Muller, W.A. (2003). Targeted recycling of PECAM from endothelial surface-connected compartments during diapedesis. Nature *421*, 748–753.

MartIn-Fontecha, A., Sebastiani, S., Höpken, U.E., Uguccioni, M., Lipp, M., Lanzavecchia, A., and Sallusto, F. (2003). Regulation of dendritic cell migration to the draining lymph node: impact on T lymphocyte traffic and priming. J. Exp. Med. *198*, 615–621.

Nakano, H., and Gunn, M.D. (2001). Gene duplications at the chemokine locus on mouse chromosome 4: multiple strain-specific haplotypes and the deletion of secondary lymphoid-organ chemokine and EBI-1 ligand chemokine genes in the plt mutation. J. Immunol. *166*, 361–369.

Nakata, T., and Hirokawa, N. (1992). Organization of cortical cytoskeleton of cultured chromaffin cells and involvement in secretion as revealed by quick-freeze, deep-etching, and double-label immunoelectron microscopy. J. Neurosci. *12*, 2186–2197.

Nourshargh, S., Hordijk, P.L., and Sixt, M. (2010). Breaching multiple barriers: leukocyte motility through venular walls and the interstitium. Nat. Rev. Mol. Cell Biol. *11*, 366–378.

Oheim, M., and Stühmer, W. (2000). Tracking chromaffin granules on their way through the actin cortex. Eur. Biophys. J. *29*, 67–89.

Ohl, L., Mohaupt, M., Czeloth, N., Hintzen, G., Kiafard, Z., Zwirner, J., Blankenstein, T., Henning, G., and Förster, R. (2004). CCR7 governs skin dendritic cell migration under inflammatory and steady-state conditions. Immunity *21*, 279–288.

Pflicke, H., and Sixt, M. (2009). Preformed portals facilitate dendritic cell entry into afferent lymphatic vessels. J. Exp. Med. *206*, 2925–2935.

Reymond, N., d'Água, B.B., and Ridley, A.J. (2013). Crossing the endothelial barrier during metastasis. Nat. Rev. Cancer *13*, 858–870.

Russo, E., Teijeira, A., Vaahtomeri, K., Willrodt, A.-H., Bloch, J.S., Nitschké, M., Santambrogio, L., Kerjaschki, D., Sixt, M., and Halin, C. (2016). Intralymphatic CCL21 Promotes Tissue Egress of Dendritic Cells through Afferent Lymphatic Vessels. Cell Rep. *14*, 1723–1734.

Saito, S., Watabe, S., Ozaki, H., Fusetani, N., and Karaki, H. (1994). Mycalolide B, a novel actin depolymerizing agent. J. Biol. Chem. *269*, 29710–29714.

Seifert, J.R.K., and Lehmann, R. (2012). Drosophila primordial germ cell migration requires epithelial remodeling of the endoderm. Development *139*, 2101–2106.

Shulman, Z., Cohen, S.J., Roediger, B., Kalchenko, V., Jain, R., Grabovsky, V., Klein, E., Shinder, V., Stoler-Barak, L., Feigelson, S.W., et al. (2011). Transendothelial migration of lymphocytes mediated by intraendothelial vesicle stores rather than by extracellular chemokine depots. Nat. Immunol. *13*, 67–76.

Südhof, T.C. (2012). Calcium control of neurotransmitter release. Cold Spring Harb. Perspect. Biol. *4*, a011353.

Takamatsu, H., Takegahara, N., Nakagawa, Y., Tomura, M., Taniguchi, M., Friedel, R.H., Rayburn, H., Tessier-Lavigne, M., Yoshida, Y., Okuno, T., et al. (2010). Semaphorins guide the entry of dendritic cells into the lymphatics by activating myosin II. Nat. Immunol. *11*, 594–600.

Tal, O., Lim, H.Y., Gurevich, I., Milo, I., Shipony, Z., Ng, L.G., Angeli, V., and Shakhar, G. (2011). DC mobilization from the skin requires docking to immobilized CCL21 on lymphatic endothelium and intralymphatic crawling. J. Exp. Med. *208*, 2141–2153.

Teijeira, A., Garasa, S., Peláez, R., Azpilikueta, A., Ochoa, C., Marré, D., Rodrigues, M., Alfaro, C., Aubá, C., Valitutti, S., et al. (2013). Lymphatic endothelium forms integrin-engaging 3D structures during DC transit across inflamed lymphatic vessels. J. Invest. Dermatol. *133*, 2276–2285.

Varadi, A., Tsuboi, T., Johnson-Cadwell, L.I., Allan, V.J., and Rutter, G.A. (2003). Kinesin I and cytoplasmic dynein orchestrate glucose-stimulated insulin-containing vesicle movements in clonal MIN6 β-cells. Biochem. Biophys. Res. Commun. *311*, 272–282.

Vestweber, D. (2015). How leukocytes cross the vascular endothelium. Nat. Rev. Immunol. *15*, 692–704.

Vigl, B., Aebischer, D., Nitschké, M., Iolyeva, M., Röthlin, T., Antsiferova, O., and Halin, C. (2011). Tissue inflammation modulates gene expression of lymphatic endothelial cells and dendritic cell migration in a stimulus-dependent manner. Blood *118*, 205–215.

Weber, M., and Sixt, M. (2013). Methods in Molecular Biology (Totowa, NJ: Humana Press).

Weber, M., Hauschild, R., Schwarz, J., Moussion, C., de Vries, I., Legler, D.F., Luther, S.A., Bollenbach, T., and Sixt, M. (2013). Interstitial dendritic cell guidance by haptotactic chemokine gradients. Science *339*, 328–332.

Wilson, R.W., Ballantyne, C.M., Smith, C.W., Montgomery, C., Bradley, A., O'Brien, W.E., and Beaudet, A.L. (1993). Gene targeting yields a CD18-mutant mouse for study of inflammation. J. Immunol. *151*, 1571–1578.

Woodfin, A., Voisin, M.-B., Beyrau, M., Colom, B., Caille, D., Diapouli, F.-M., Nash, G.B., Chavakis, T., Albelda, S.M., Rainger, G.E., et al. (2011). The junctional adhesion molecule JAM-C regulates polarized transendothelial migration of neutrophils in vivo. Nat. Immunol. *12*, 761–769.

Zhu, X., Hu, R., Brissova, M., Stein, R.W., Powers, A.C., Gu, G., and Kaverina, I. (2015). Microtubules negatively regulate insulin secretion in pancreatic β cells. Dev. Cell *34*, 656–668.

Cell Reports, Volume *19*

Supplemental Information

Locally Triggered Release of the Chemokine CCL21 Promotes Dendritic Cell Transmigration across Lymphatic Endothelia

Kari Vaahtomeri, Markus Brown, Robert Hauschild, Ingrid De Vries, Alexander Franz Leithner, Matthias Mehling, Walter Anton Kaufmann, and Michael Sixt

Figure S1

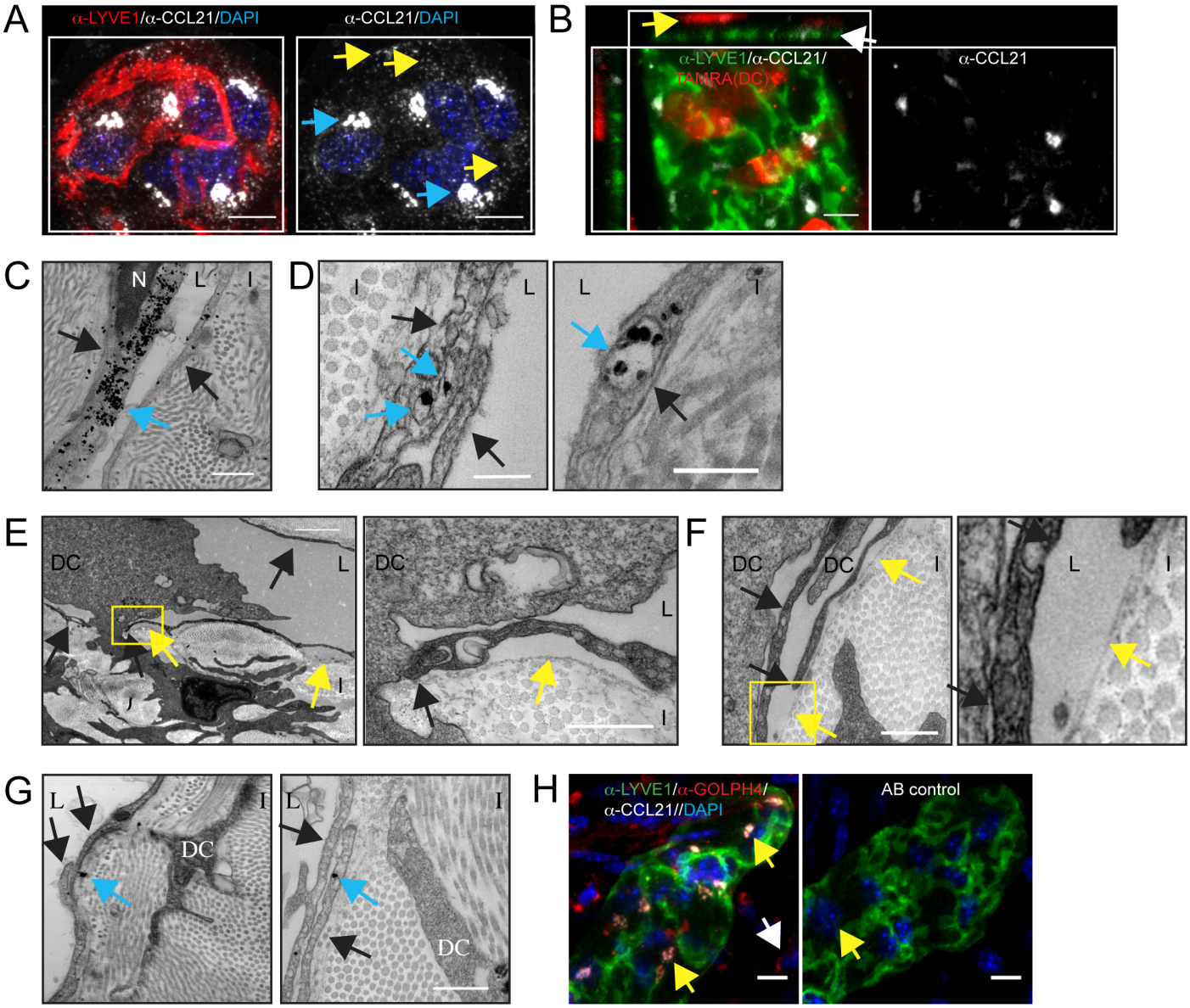
A
α-LYVE1/α-CCL21/DAPI
α-CCL21/DAPI
B
α-LYVE1/α-CCL21/
TAMRA(DC)
α-CCL21
C
N
L
I
D
I
L
L
I
E
DC
L
I
DC
L
I
F
DC
DC
I
L
I
G
L
I
DC
L
I
DC
H
α-LYVE1/α-GOLPH4/
α-CCL21//DAPI
AB control

Figure S1. CCL21 localization and DC-LEC interaction in dermal tissue. Related to Figure 1. (A) A blind end of mouse dermal lymphatic capillary stained for LYVE1 (red), CCL21 (white) and nucleus (DAPI, blue). Yellow arrows indicate some of the intracellular CCL21 vesicles and blue arrows Golgi deposits. **(B)** Staining of LYVE1 (green) and CCL21 (white) of the wild type dermis invaded by TAMRA labeled *Ccr7*$^{-/-}$ DCs (red). Yellow arrow depicts the DC and white arrow the lymphatic capillary in the orthogonal image. **(C-D and G)** Transmission electron micrographs of CCL21 staining of dermis. Black arrows indicate LECs and blue arrow silver-amplified CCL21 immunogold label, which are enriched (C) perinuclearly and (D) in vesicles, but (G) not enriched at the site of non-interacting DC and LEC. Interstitium (I), LEC nucleus (N), lumen (L) and DC are marked. **(E-F)** Transmission electron micrographs of LEC transmigrating DC. Black arrows indicate the LECs, yellow arrows the basement membrane at the site of detached LEC. Figures on the right show a zoom-in of the boxed region. Interstitium (I), lumen (L) and DC are marked. **(H)** On the left, a blind end of mouse dermal lymphatic capillary stained with anti-Lyve1 (green), anti-GOLPH4 (red), anti-CCL21 (white) and DAPI (nuclei, blue) and the appropriate secondary antibodies. On the right, an identical staining except the primary antibodies for GOLPH4 and CCL21 were omitted to control the specificity of the primary antibodies. Scale bars 10μm in (A-B), in (C) 500nm, in (D) 200nm, in (E) 2μm and 500nm in the inset, in (F) 500nm, in (G) 500nm and in (H) 10μm.

Figure S2

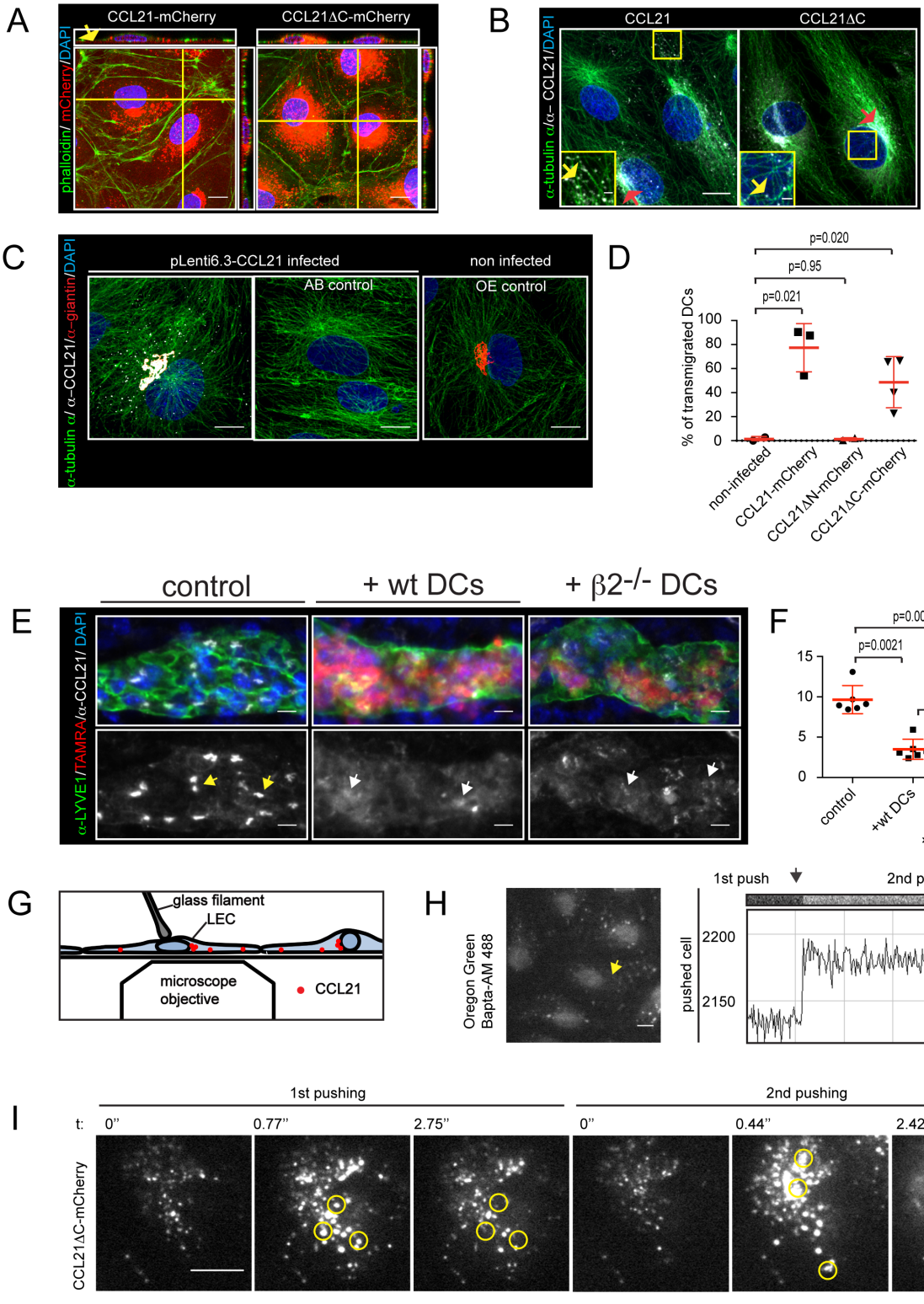
A
CCL21-mCherry
CCL21ΔC-mCherry
phalloidin/ mCherry/DAPI
B
CCL21
CCL21ΔC
α-tubulin α/α– CCL21/DAPI
C
pLenti6.3-CCL21 infected
non infected
AB control
OE control
α-tubulin α/ α–CCL21/α–giantin/DAPI
D
p=0.020
p=0.95
p=0.021
% of transmigrated DCs
100
80
60
40
20
0
non-infected
CCL21-mCherry
CCL21ΔN-mCherry
CCL21ΔC-mCherry
E
control
+ wt DCs
+ β2-/- DCs
α-LYVE1/TAMRA/α-CCL21/ DAPI
F
p=0.0012
p=0.0021
p=0.051
15
10
5
0
control
+wt DCs
+β2-/- DCs
G
glass filament
LEC
microscope objective
CCL21
H
Oregon Green Bapta-AM 488
1st push
2nd push
pushed cell
2200
2150
I
1st pushing
2nd pushing
t:
0”
0.77”
2.75”
0”
0.44”
2.42”
CCL21ΔC-mCherry

Figure S2. CCL21 localization in primary LEC cultures (related to figure 2), and effect of integrin β2$^{-/-}$ DC-LEC interaction in dermis or mechanical stimulus *in vitro* on CCL21 dispersion/secretion (related to figure 4). (A) Phalloidin (green) and DAPI (blue) staining of CCL21-mCherrry or CCL21ΔC-mCherrry (red) expressing LECs. Yellow lines indicate the plane of orthogonal sections and yellow arrow in the orthogonal section the extracellular CCL21-mCherry anchored on the cell culture dish surface. **(B)** Staining of tubulin-α (green), CCL21 (white) and nucleus (DAPI, blue) in LECs expressing non-tagged CCL21 or CCL21ΔC. Red arrows indicate the Golgi localized depots of CCL21 and yellow arrows in zoom-in boxes the MT associated CCL21. **(C)** Staining of tubulin-α (green), CCL21 (white), giantin (red) and nuclei (blue) in CCL21 overexpressing (OE) LECs (on the left) or non-infected LECs (on the right, OE control). Picture in the middle shows an antibody control, in which CCL21 and giantin primary antibodies were omitted. **(D)** Quantification of DC transmigration on non-infected, CCL21-mCherry, CCL21 ΔN-mCherry or CCL21 ΔC-mCherry expressing monolayers. For CCL21-mCherry and CCL21 ΔC-mCherry dot blot graph shows mean +/- SD of pooled samples from 3 independent experiments, n=3 or 4, respectively. Two of these independent experiments included non-infected or CCL21 ΔN-mCherry expressing monolayers for which n=2. Data is presented as percentage of transmigrated DCs. See video 4. **(E)** LYVE1 (green), CCL21 (white) and nuclei (DAPI, blue) of the ear dermis after 7h in presence or absence (control) of TAMRA labeled wild type or integrin β2$^{-/-}$ (β2$^{-/-}$) DCs (red). White arrows indicate dispersion of CCL21 (yellow arrow in control). **(F)** Dot blot graph shows ratio of signal in high intensity CCL21 depots to CCL21 in other areas of LECs. Columns represent mean values +/- SD of control (n=6), + wild type DC (n=6) or + integrin β2$^{-/-}$ (β2$^{-/-}$) DC (n=7) samples of approximately 300μm long lymphatic vessel stretches. **(G)** Schematic depicts experimental set up, in which the basolateral side of a LEC is imaged with TIRF microscopy while, due to limitations of the setup, the apical (luminal) side, instead of the physiological basolateral side, of the LEC is pushed by micromanipulator guided glass filament. **(H)** A still image of time-lapse imaged and 10μM Oregon Green BAPTA-AM (white) treated LEC monolayer. A kymograph and corresponding line graph of Oregon Green BAPTA-AM intensity shows the Ca fluxes for the cytoplasmic region of the pushed cell (yellow arrow). **(I)** Time-lapse imaging of 2 consecutive pushes of a single LEC in a monolayer expressing CCL21ΔC-mCherry (white). Pushing occurred at 2nd frames as seen by more intense mCherry signal. At 3rd frames many of the vesicles have been secreted. Some of the sites of vesicle secretion are highlighted prior and subsequent to the secretion with yellow circles. Scale bars are in (A-C, E, H-I) 10μm and 2μm in insets in (B).

Supplemental experimental procedures

Generation and labeling of bone marrow derived dendritic cells

For generation of mature DCs, bone marrow was extracted from femur and tibia of 8-12 weeks old C57BL/6J mice and cultured in R10 culture medium (RPMI1640 culture medium supplemented with 10% fetal calf serum, L-Glutamin and Penicillin/Streptomycin, all from Gibco) and GM-CSF hybridoma supernatant. Day 8 DCs were activated for 20h with 200ng/ml LPS (Sigma L2654). Activated DCs were labeled for 15' at room temperature with 6.7µM 5-(and-6-) carboxytetramethylrhodamine, succimidyl ester (TAMRA; molecular probes, Life Technologies) in phosphate buffered saline (PBS). The staining reaction was terminated by addition of R10 followed by centrifugation and resuspension of cells in R10. Prior to experimentation DCs were cultured for 1h at 37°C and 5% CO_2.

Ear sheet staining

For Fig. 1B-C, S1A and S2E fixed ear sheets were permeabilized with 0.15% Triton x-100 in PBS for 15', blocked with 1% bovine serum albumin (BSA, Sigma) in PBS for 1h and stained with anti mouse LYVE1 (R&D, MAB2125) and anti mouse CCL21 antibodies (R&D, BAF457) in the blocking buffer. For Fig. 1A and S1H ear sheets were permeabilized with 0.5% Triton x-100, blocked with 3% non-fat milk in 0.5% Triton x-100 in PBS for 1h and stained with anti mouse GOLPH4 (Abcam ab28049), LYVE1 (R&D, MAB2125) and CCL21 (R&D BAF457) antibodies diluted in blocking buffer. Fluorochrome conjugated secondary antibodies (α-rat Alexa fluor 488, Jackson Immunoresearch 712-546-150; α-rat Dylight 549, Jackson Immunoresearch 712-506-150; α-rabbit Cy3, Jackson immunoresearch, 111-165-144) and streptavidin (alexa fluor 647, Jackson Immunoresearch, 016-600-084) were diluted in 1% BSA in PBS. Finally, ear sheets were counter-stained with DAPI (Life Technologies, D1306). Imaging of ear sheets was carried out with a LSM700 upright microscope equipped with a Plan-Apochromat 20x water (numerical aperature 1.0) DIC objective and Zen 2011 software.

Transmission electron microscopy

For ultrastructural analysis (Fig. 4A and S1E-F), ears were fixed with half-Karnovsky's 2.5% glutaraldehyde (GA) and 2% PFA in 0.1M phosphate buffer (PB). Samples were treated with 2% osmium tetroxide in PB (40' at room temperature in the dark) and contrast enhanced by means in 1% uranyl acetate in 50% ethanol (30' at room temperature) and 2.6% lead nitrate in sodium citrate (5' at room temperature). Samples were then flat-embedded in epoxy resin (Durcupan® ACM) on greased glass slides. Regions of interest were dissected and re-embedded in epoxy resin. Serial ultrathin sections (70-80 nm) were cut with an ultramicrotome (Leica Microsystems UC7) and collected on formvar-coated copper slot grids.

For immunolocalization of proteins (Fig. 1E, 4B and S1C, D and G) a pre-embedding immunometal labeling technique (immunogold plus silver amplification) was applied. Ears were fixed with 4% PFA and 0.05% GA in PB for 25' at room temperature, permeabilized with 0.15% Triton x-100 and incubated in 50mM glycine in PBS for quenching of free aldehyde groups, followed by incubation in 1% BSA in PBS for blocking of nonspecific binding sites. Samples were immunostained with biotinylated anti CCL21 (R&D, BAF457) and nanogold®-streptavidin (Nanoprobes Inc.). Nanogold particles were amplified with silver using the HQ SilverTM Enhancement kit (Nanoprobes Inc.) for 6-8' at room temperature under light microscopy control. Samples were washed in MilliQ water and postfixed in 2% GA in PB prior to embedding in epoxy resin. Specificity of immunodetection was controlled and confirmed omitting primary antibodies with following application of the nanogold®-streptavidin. Ultrathin sections were cut at 80 nm and examined in a TECNAI 10 transmission electron microscope operated at 80 kV, equipped with a Morada CCD camera (Soft Imaging Systems). Alternatively, sections were cut at 250 nm, collected on formvar-coated 100-line bar grids, carbon coated (6 nm thickness) and observed under a Jeol JEM 2800 operated at 200 kV in STEM bright-field mode.

DNA constructs

For cloning of *Ccl21*, mouse spleen mRNAs were isolated (RNeasy mini kit, Qiagen) and converted to cDNA by reverse transcriptase reaction (Maxima H minus first strand cDNA synthesis kit, Thermo). Using cDNA pool as a template, *Ccl21* was amplified via PCR reaction (Phusion, Thermo scientific) with a 5'-cac ctc gag cat ggc tca gat gat gac tct g-3' forward and either with 5'- tga att cta tcc tct tga

ggg ctg tgt c -3' (with stop codon) or 5'- tga att cgc tcc tct tga ggg ctg tgt c -3' (without a stop codon) reverse primers followed by directional TOPO cloning (pENTR/D-TOPO, Invitrogen). To fuse *Ccl21* and mCherry, both pENTR/D-TOPO-Ccl21 and mCherry, which was amplified from pBabe-TetCMV-puro-mCherry-PA-Rac1 (Addgene, forward 5'-taagcagaattcaaagctggctagcatggtgag-3' and reverse 5'-tgcttagaattcttacttgtacagctcgtccatgcc-3' primers), were cut with EcoR1 and ligated with T4 ligase (Express link T4 ligase, Invitrogen) to yield pENTR/D-TOPO-Ccl21-mCherry. To delete the N- (amino acids 1-23) or C-terminus (amino acids 99-133) of the CCL21 we carried out a PCR based site directed mutagenesis (Phusion, Thermo scientific). For N-terminal deletion 5' phosphorylated 5'- agt gat gga ggg ggt cag gac tgc tgc ctt-3' forward and 5'- cat gct cga ggt gaa ggg ggc ggc c-3' reverse primers and for C-terminal deletion either 5'-gcg aat tca aag ctg gct agc atg gtg agc-3' (for pENTR/D-TOPO-Ccl21-mCherry) or 5'- tag aat tca aag ggt ggg cgc gcc-3' (for pENTR/D-TOPO-Ccl21-STOP) forward and 5'-ttt ccc tgg ggc tgg agg ctg gtc-3' reverse primers were used for amplification of a truncation mutant via PCR, which was followed by ligation. Finally, pLenti6.3-Ccl21-mCherry, pLenti6.3-Ccl21ΔC-mCherry, pLenti6.3-Ccl21ΔN-mCherry, pLenti6.3-Ccl21 and pLenti6.3-Ccl21ΔC were created by a LR-reaction (Invitrogen) between the pLenti6.3 (Invitrogen) and the above-described pENTR/D-TOPO vectors.

To obtain pLenti6.3-Lifeact-EGFP, attB1/2 gateway forward 5' ggg gac aag ttt gta caa aaa agc agg cta cca tgg gtg tcg cag att tga tc 3' and reverse 5' ggg gac cac ttt gta caa gaa agc tgg gtt tac ttg tac agc tcg tcc atg 3' primers were designed to amplify the DNA sequence via PCR from the plasmid described earlier (Riedl et al., 2008). The PCR product was then recombined into the pDONR221 donor vector (Invitrogen) via gateway BP reaction. The resulting plasmid was then used in a LR gateway reaction to obtain the plenti6.3 expression vector.

To obtain pLenti6.3-EGFP-tubulin α , EGFP-tubulin α 1B was amplified from EGFP-tubulin α 1B expression plasmid (a kind gift from professor Vic Small) with the attB1/2 gateway forward 5'-ggg gac aag ttt gta caa aaa agc agg ctt cac cat ggt gag caa ggg c -3' and reverse 5'- ggg gac cac ttt gta caa gaa agc tgg gtc gga tcc tta gta ttc ctc tcc ttc -3' primers. The PCR product was then recombined into the pDONR221 donor vector (Invitrogen) via gateway BP reaction. The resulting plasmid was then used in a LR gateway reaction to obtain the plenti6.3 expression vector.

Identification of putative nuclear localizing signal

cNLS mapper (http://nls-mapper.iab.keio.ac.jp/cgi-bin/NLS_Mapper_form.cgi) (Kosugi et al., 2009) was used to search the mature (the same as CCL21 ΔN) mouse CCL21 sequence for putative nuclear localization signal. A putative non-conserved bipartite nuclear localization signal covering aa's 21-50 was identified.

Virus production

Viruses encoding pLenti6.3-Ccl21, pLenti6.3-Ccl21ΔC, pLenti6.3-Ccl21-mCherry, pLenti6.3-Ccl21ΔC-mCherry, pLenti6.3-Ccl21ΔN–mCherry, pLenti6.3-Lifeact –EGFP and pLenti6.3-EGFP-tubulin α were produced in LentiX-293 packaging cells (Chemicon, Darmstadt, Germania) according to the protocols of Functional Genomics Unit of the University of Helsinki (http://www.helsinki.fi/fugu/).

LEC culture and infections

Primary human juvenile foreskin dermal lymphatic endothelial cells (LEC, C-12216, Promocell) were cultured in ready-to-use FCS and growth factor supplemented endothelial cell growth medium MV2 (Promocell, www.promocell.com, C-22022) in the absence of antibiotics. The LECs were checked for the expression of the CCL21 (R&D, MAB366) and podoplanin (Breiteneder-Geleff et al., 1999) (the antibody was a kind gift of Dontscho Kerjaschki). Small amounts of endogenous CCL21 were found confined in Golgi apparatus as reported earlier (Johnson and Jackson, 2010). Cells were used for experimentation at passages 4-6 and plated on 0.1% gelatin coated 1.5cm^2 large wells with #1.5 thick coverslip bottom or 24-well plates (day 0) and infected with 1:20 diluted viruses in the MV2 media in the presence of 9 μg/ml polyprene (Sigma) for 6-8h at day 1. The media was changed once/day and the cells were used for experimentation at day 3-5, 1 day subsequent to reaching full confluency.

Staining of LECs
The fixed samples were permeabilized with 0.15% Triton x-100 in PBS for 10', blocked with 1% BSA in PBS for 1h and stained with phalloidin (Alexa fluor 488, A12379 Thermo Fisher scientific) and anti human tubulin α (AbD Serotec, MCA77G), anti mouse CCL21 (biotinylated, R&D BAF457) and anti human giantin (Abcam ab24586) specific antibodies diluted in the blocking buffer. Fluorochrome conjugated secondary antibodies (α-rat alexa fluor 488, Jackson immunoresearch 712-546-150; α-rabbit alexa fluor 647, Jackson immunoresearch, 711-606-152) and streptavidin (alexa fluor 647, Jackson immunoresearch, 016-600-084) were diluted in 1% BSA in PBS. Finally, the LECs were counterstained with DAPI (Life Technologies, D1306). Stained cells were imaged with a Zeiss LSM700 inverted microscope equipped with a Plan-APOCHROMAT 63x/1.4 Oil objective and Zen 2011 software or with a LSM700 upright microscope equipped with Plan-Apochromat 20x water (numerical aperature 1.0) and 40x oil (numerical aperature 1.4) DIC objectives and Zen 2011 software.

Measurements of mCherry signals of the culture supernatant
The LEC culture supernatant was centrifuged at 500RCF for 6' and 200µl of the supernatant was transferred to black 96-well plates (Greiner). Fluorescence was measured with a Synergy H1 plate reader (Biotek, excitation 587nm and emission 620nm).

For the experiment shown in Fig. 2B, each of the cultures were stained with DAPI and imaged with Zeiss LSM700 inverted microscope equipped with Plan apochromat 20x dry (numerical aperature 0.8) objective and Zen 2011 software followed by quantification of infection efficiencies to normalize CCL21-mCherry and CCL21ΔC-mCherry levels relative to CCL21ΔN-mCherry. Finally, results were normalized to the background fluorescence of non-infected LEC culture supernatant, which was set as 1. Serial dilution of a 48h supernatant sample from CCL21ΔC -mCherry expressing LECs showed a linear increase in fluorescence upon increased amount of CCL21ΔC-mCherry supernatant.

Microscope setup for live TIRF imaging of CCL21-mCherry positive vesicles
Infected LECs were time-lapse imaged with an Olympus IX 83 microscope equipped with a Hamamatsu EMCCD C9100-13 camera, cell TIRF, UAPON 100X OTIRF objective (numerical aperature of 1.49), xcellence rt 2.0 software and an incubator with +37C and 5% CO_2 atmosphere.

Microscope setup for *In vitro* DC transmigration assay
Immediately after addition of DCs, phase contrast time-lapse imaging at 20'' frame frequency was started with a Leica DM IL LED microscope equipped with a S40/0.45 condensor, phase contrast, modulation and Leica HI PLAN CY 10x (numerical aperature 0.25) objective and an incubator with 37°C and 5% CO_2 atmosphere.

LEC Ca sensor assays
For the co-incubation of LECs and DCs, the TAMRA labeled DCs were washed twice with PBS after terminating the TAMRA reaction with RPMI1640 supplemented with 10% FCS, and resuspended in MV2 culture media (Promocell) supplemented with L-glutamin but devoid of growth factor supplement (Called hereafter MV2–). After preparing the DCs, the LECs were loaded either with fresh MV2– (control), MV2– DC conditioned supernatant, MV2– media with 100000 DCs or MV2– media with 100000 Mycalolide B (Santa Cruz), an irreversible actin depolymerizing agent (Hori et al., 1993; Saito et al., 1994), pre-treated 100000 DCs. The conditioned supernatant was produced by incubating 100000 DCs in MV2– media for 40' followed by centrifugation. Media with DCs was produced by adding 100000 DCs to MV2– media, which were co-incubated 20' prior to adding on the cells. Mycalolide B treated DCs were produced by incubating TAMRA labeled DCs in 1.0µM Mycalolide B for 15' followed by 3x washing with PBS and resuspension in MV2– media for 20' before loading on the LECs. The lack of actin dependent protrusion was confirmed with phase contrast microscopy.

Control, conditioned, DC containing or Mycalolide B pre-treated DC containing MV2– media (Promocell) was carefully added on a 1.5cm^2 well or Ibidi 8-well glass bottom µ-slide of day 4-5 confluent CCL21 overexpressing LEC monolayer, which had prior to loading been washed twice with MV2– media, treated for 50' with 10µM Oregon Green BAPTA-AM Ca sensor (Life Technologies, O6807) and washed twice with MV2– culture media. The time-lapse imaging was started 10' after loading the DCs at 2.2'' frame interval with a Nikon Eclipse Ti microscope equipped with Lumencolor

light engine, Hamamatsu ORCA R2 (model C10600) and EMCDD C9100-02 cameras, 10x PLAN FLUOR Ph1 DL (numerical aperature 0.3) and 20x PLAN FLUOR (numerical aperature 0.5) objectives, NIS-Elements AR 4.00.08 software and an incubator with 37°C and 5% CO_2 atmosphere. For the cell population analysis (Fig. 4E) imaging lasted for 10' and the number of LECs displaying transient Ca peaks was quantified from acquired videos.

Mechanical pushing of the cells

For mechanical pushing of the CCL21ΔC-mCherry expressing_LECs a glass pipette was heated and pulled into a thin filament. The tip of the glass filament was melted into a solid microsphere and then mounted on a micrometer driven x/y/z translation stage which itself was attached to the Olympus IX 83 microscope stage. In transmitted light the microsphere acted as lens which produced a bright focus which allowed for precise positioning of the microsphere above the nucleus of the cell of interest without touching the cell. Subsequently the microsphere was carefully lowered using the z-axis until a pushing force was applied to the cell. Concomitantly with pushing, the cells were time lapse imaged with_Olympus IX 83 microscope equipped with Hamamatsu EMCCD C9100-13 camera, cell TIRF, xcellence rt 2.0 software and an incubator with +37C and 5% CO^2 atmosphere. The TIRF mode and UAPON 100X OTIRF objective (numerical aperature of 1.49) were used to image the CCL21-mCherry secretion.

For monitoring of Ca fluxes upon mechanical pushing, the CCL21ΔC-mCherry expressing LECs were incubated with 10µM oregon green BAPTA-AM in supplemented MV2 culture media (Promocell, see cell culture) for 1h, washed twice with PBS and incubated with supplemented MV2 culture media (Promocell). The critical angle setting and UAPON 0340 40x objective (numerical aperature 1.15) were used to allow imaging of the whole oregon green BAPTA-AM treated LECs in Z-direction. The Ca sensor intensity (oregon green BAPTA-AM) kymographs were created and analyzed with FiJi software.

Image analysis

CCL21-mCherry vesicles were tracked automatically using ImarisTrack (Imaris 7.4, BITPLANE). The resulting tracks were filtered by track length and track displacement and then manually classified and color-coded accordingly (see Fig. 2C).

To quantify the dispersion of LEC intracellular CCL21 upon DC transmigration (Fig. 1C-D and S2E-F), 300µm long stretches of lymphatic capillary in confocal images were presegmented using Ilastik (ilastik.org) and cleaned up manually. The resulting binary images were eroded to avoid edge effects and converted into masks. Likewise perinuclear CCL21 regions were segmented employing intensity based thresholding and converted into masks. Using Fiji a representative background region was drawn manually and the raw CCL21 intensities of the background (non-specific staining, detection offset)(I_B), perinuclear region (I_PN) and rest of LV (I_LV) were measured. The enrichment in the perinuclear region is then given by: (I_PN-I_B)/(I_LV-I_B).

Fiji software was also used for brightness/contrast adjustment of images and videos and for length measurements of LECs in transmission electron micrographs.

References

Breiteneder-Geleff, S., Soleiman, A., Kowalski, H., Horvat, R., Amann, G., Kriehuber, E., Diem, K., Weninger, W., Tschachler, E., Alitalo, K., et al. (1999). Angiosarcomas Express Mixed Endothelial Phenotypes of Blood and Lymphatic Capillaries. The American Journal of Pathology *154*, 385–394.

Hori, M., Saito, S.-Y., Shin, Y.Z., Ozaki, H., Fusetani, N., and Karaki, H. (1993). Mycalolide-B, a novel and specific inhibitor of actomyosin ATPase isolated from marine sponge. FEBS Letters *322*, 151–154.

Johnson, L.A., and Jackson, D.G. (2010). Inflammation-induced secretion of CCL21 in lymphatic endothelium is a key regulator of integrin-mediated dendritic cell transmigration. International Immunology *22*, 839–849.

Kosugi, S., Hasebe, M., Tomita, M., and Yanagawa, H. (2009). Systematic identification of cell cycle-dependentyeast nucleocytoplasmic shuttling proteinsby prediction of composite motifs. Proceedings of the National Academy of Sciences *106*, 10171–10176.

Riedl, J., Crevenna, A.H., Kessenbrock, K., Yu, J.H., Neukirchen, D., Bista, M., Bradke, F., Jenne, D., Holak, T.A., Werb, Z., et al. (2008). Lifeact: a versatile marker to visualize F-actin. Nat Meth *5*, 605–607.

Saito, S.-Y., Watabe, S., Hiroshi, O., Fusetani, N., and Karaki, H. (1994). Mycalolide B, a Novel Actin Depolymerizing Agent*. The Journal of Biological Chemistry *269*, 29710–29714.